Uplink Throughput Performance of Single-Carrier MIMO Spatial Multiplexing in Distributed Antenna Network

Tetsuya YAMAMOTO[1] and Fumiyuki ADACHI[2]
[1,2]Dept. of Electrical and Communication Engineering, Graduate School of Engineering, Tohoku University
6-6-05 Aza-Aoba, Aramaki, Aoba-ku, Sendai, 980-8579 Japan
[1]yamamoto@mobile.ecei.tohoku.ac.jp, [2]adachi@ecei.tohoku.ac.jp

***Abstract*—Multiple-input multiple-output (MIMO) spatial multiplexing achieves very high spectrum efficient signal transmissions in a cellular network (CN). However, this is only possible when the received signal-to-interference plus noise power ratio (SINR) is high enough. In a conventional CN, multiple antennas are co-located at each based station (BS) and hence, the throughput of a mobile terminal (MT) close to the cell edge significantly degrades due to reduced received SINR. Distributed antenna network (DAN), in which many antennas are spatially distributed over the cell, can solve this problem. In DAN, since some antennas can always be visible from an MT with a high probability, the received SINR can be increased over the entire cell. In this paper, we investigate the spatial distribution of the throughput of single-carrier (SC) MIMO packet transmission using hybrid automatic repeat request (HARQ) and a near maximum likelihood signal detection in DAN. First, we evaluate, by computer simulation, the spatial distribution of the uplink throughputs in a single-cell environment and show that DAN can achieve higher throughput than CN over the entire cell. Furthermore, we discuss the impact of the frequency reuse factor on the uplink throughput in a multi-cell environment and show that DAN can reduce the frequency reuse factor and achieves higher spectrum efficiency than CN.**

Keywords-component; Distributed antenna, MIMO spatial multiplexing, single-carrier, near maximum likelihood detection

I. INTRODUCTION

In next generation mobile data communication systems, broadband data services are demanded. However, the available bandwidth is limited. Multi-input multi-output (MIMO) spatial multiplexing [1] achieves high data rate without increasing the signal bandwidth. For uplink (mobile terminal (MT)-to-base station (BS)) transmissions, single-carrier (SC) transmission is suitable because of its lower peak-to-average power ratio (PAPR) property [2, 3] than multi-carrier transmission, e.g., orthogonal frequency division multiplexing (OFDM) [4]. Hence, SC-MIMO has been adopted as the uplink transmission technique for the 3rd generation partnership project long term evolution (3GPP LTE) systems [5].

Since the wireless channel becomes severely frequency-selective as the transmission data rate increases [6], SC-MIMO suffers not only from inter-antenna interference (IAI) but also from inter-symbol interference (ISI) arising from the severe frequency-selectivity of the channel. QR decomposition and M-algorithm based near maximum likelihood (ML) block detection (QRM-MLBD) [7-9] significantly improves the transmission performance of SC-MIMO systems in a frequency-selective fading channel with significantly lower computational complexity compared to full ML detection. It was shown in [9] that QRM-MLBD achieves a significantly higher throughput than the well-known minimum mean square error based linear detection (MMSED), in particular, when high level modulation and high rate coding are used.

The broadband wireless channel is characterized not only by frequency-selective fading but also by path loss and shadowing loss [6]. In conventional cellular networks (CNs), multiple antennas for spatial multiplexing are co-located at each BS, and therefore, the received signal power of an MT near the cell edge often drops. Moreover, in the CN where the same frequency is reused in spatially separated cells to efficiently utilize the limited frequency bandwidth, the receiver suffers the co-channel interference (CCI) from neighboring cells. As a consequence, the received signal-to-interference plus noise power ratio (SINR) of an MT near the cell edge significantly drops, and accordingly the transmission rate significantly degrades even if MIMO spatial multiplexing is used. The distance between each co-channel cells has to be long to improve the received SINR. However, this reduces the bandwidth to be allocated to each cell for the given system bandwidth (resulting in lower spectrum efficiency defined as bps/Hz/cell).

A distributed antenna network (DAN) [10-12], in which each MT is served by using multiple distributed antennas close to it, is a promising solution to the above issue. In DAN, the conventional BS is replaced by the signal processing center (SPC) and many antennas are spatially distributed over the cell so that some antennas can always be visible from an MT with a high probability to make the received SINR sufficiently high even near the cell edge. Antennas are connected to nearby SPC by means of optical fiber links and a number of distributed antennas cooperate and act as distributed MIMO multiplexing to improve the transmission rate and the spectral efficiency. In [13, 14], we investigated the channel capacity distribution of DAN-MIMO spatial multiplexing and showed that DAN achieves high channel capacity over the entire cell. We also showed that in multi-cell environment, DAN allows smaller frequency reuse factor and achieves higher spectrum efficiency than CN.

Most of previous works on DAN-MIMO spatial multiplexing focused on the channel capacity analysis. The performance of DAN-MIMO spatial multiplexing with hybrid automatic repeat request (HARQ) and practical signal detection scheme has not been fully investigated. In this paper, we investigate the uplink throughput of DAN using SC-MIMO packet transmission employing type II HARQ [15, 16] and QRM-MLBD. Among many HARQ protocols, type II HARQ is promising. In type II HARQ, an information packet is first transmitted. If it is erroneously received, a part of redundancy bits is transmitted. Since the first packet transmission is uncoded (or coded with high coding rate), the throughput performance of DAN using

SC-MIMO HARQ with QRM-MLBD is expected to be more effective than MMSED.

The rest of the paper is organized as follows. In Section II, system model of DAN uplink is presented. Section III describes the SC-MIMO signal transmission system model and QRM-MLBD. In Section IV, we present the simulation results. First, we discuss the uplink throughput distribution in a single-cell environment to show that DAN achieves higher throughput over the entire cell and significantly reduces the transmit power required for achieving the required throughput compared to CN. Then, we discuss the uplink throughput distribution in a multi-cell environment and show that DAN significantly improves the spectrum efficiency than CN. Finally, in Section V, we conclude the paper.

II. System Model

A. Channel Model

The channel is characterized by distant-dependent path loss, log-normally distributed shadowing loss and frequency-selective fading. We consider the channel between n-th transmit antenna (n=0~N_t–1) at the MT and m-th received distributed antenna (m=0~N_r–1). Assuming a frequency-selective channel composed of L distinct paths, the channel impulse response is expressed as

$$h_{m,n}(\tau) = \sqrt{r_m^{-\alpha} \cdot 10^{-\eta_m/10}} \sum_{l=0}^{L-1} h_{m,n,l}\,\delta(\tau - \tau_{m,n,l}), \qquad (1)$$

where r_m=R_m/R is the normalized distance between the MT and m-th distributed antenna with R_m and R being the distance between the MT and m-th distributed antenna and cell radius, respectively. α is the path loss exponent and η_m is the shadowing loss in dB having zero-mean and standard deviation σ. $h_{m,n,l}$ and $\tau_{m,n,l}$ are respectively the complex-valued path gain with $E[\sum_{l=0}^{L-1}|h_{m,n,l}|^2]=1$ and the time delay of the l-th path.

B. Network Model

1) Single-cell environment

Figure 1 illustrates the models of DAN and CN in a single-cell environment. The single MT which is equipped with N_t transmit antennas is considered. In the case of the DAN, N_{total}=7 antennas are distributed over an entire cell and N_r antennas are selected among N_{total} antennas, based on the local average received signal power $r_m^{-\alpha} \cdot 10^{-\eta_m/10}$, m=0~N_{total}–1 (i.e., based on path loss plus shadowing loss). In DAN, distributed antennas are equidistantly distributed along the circle of radius 2R/3. On the other hand, in the case of the CN, N_{total} antennas are localized at the BS and N_r antennas are selected based on the instantaneous received signal power $\sum_{l=0}^{L-1}|h_{m,n,l}|^2$.

2) Multi-cell environment

Figure 2 illustrates an example of multi-cell model when the frequency reuse factor F=3. The center cell (c=0) is assumed to be the cell of interest. There are 6 CCI cells in the first tier and 12 CCI cells in the second tier (c=1~18). The layout of distributed antennas is same as in Fig. 1. The single MT which is equipped with N_t transmit antennas is considered in each cell.

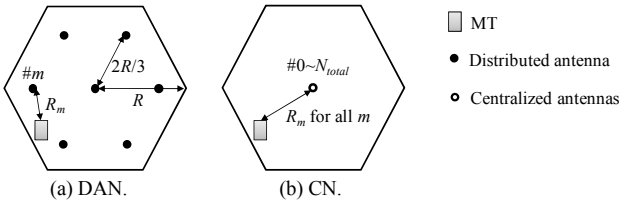

(a) DAN. (b) CN.

Figure 1. Models of DAN and CN.

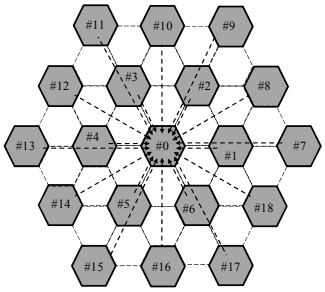

Figure 2. Multi-cell model (F=3).

III. SC-MIMO HARQ Using QRM-MLBD in Uplink DAN

A. Transmission System

Figure 3 illustrates the transmitter and receiver structure of SC-MIMO HARQ using QRM-MLBD. In this paper, we consider the HARQ type II S-Px [16] and turbo coding with rate R_c=1/3. The turbo encoder outputs the systematic bit sequence and two parity bit sequences. These sequences are punctured into (x+1) sequences (including systematic bit sequence). For the first (0-th) transmission, only the systematic bit sequence is transmitted. At the receiver, data decision and error detection are performed. If any error is detected in the received packet, second transmission is requested from the receiver by sending a negative acknowledgment (NACK) signal. When the NACK signal is received at the transmitter, the second packet (consisting of the punctured parity bit sequence) is transmitted. At the receiver, turbo decoding is carried out by using the first and second received packets. If any error is detected after turbo decoding, the NACK signal is transmitted again. One of the punctured parity bit sequences is transmitted each time the NACK signal is received at the transmitter until the x-th packet transmission. After the x-th packet transmission, the same packet is retransmitted.

At the transmitter, after turbo coding and puncturing, the coded bit sequence is stored in the transmitter buffer. The coded bit sequence is transformed into a data-modulated symbol sequence. Then, the data-modulated symbol sequence is serial-to-parallel (S/P) converted to N_t parallel symbol sequence, each to be transmitted from a different transmit antenna and each parallel symbol sequence is divided into a sequence of symbol blocks of N_c symbols each. The data symbol block of n-th transmit antenna can be expressed using the vector form as $\mathbf{d}_n=[d_n(0),\ldots,d_n(t),\ldots,d_n(N_c-1)]^T$, where $(.)^T$ expresses the transposition. The training sequence (TS) inserted SC block transmission [17, 18] is used instead of well-known cyclic prefix inserted SC (CP-SC) transmission as the use of TS can reduce the detection complexity of QRM-MLBD [8, 9]. Before the transmission, the TS of length N_g symbols is appended at the end of each block. The block

$\mathbf{s}_n=[s_n(0),\ldots,s_n(t),\ldots,s_n(N_c+N_g-1)]^T$ to be transmitted is expressed using the vector form as

$$\begin{aligned}\mathbf{s}_n &= [d_n(0),...,d_n(N_c-1),u_n(0),...,u_n(N_g-1)]^T \\ &= [\mathbf{d}_n{}^T \quad \mathbf{u}_n{}^T]^T\end{aligned}, \tag{2}$$

where $\mathbf{u}_n=[u_n(0),\ldots,u_n(t),\ldots,u_n(N_g-1)]^T$ denotes the TS vector which is identical for all blocks.

A superposition of N_t transmitted blocks is received by N_r distributed antennas. The received signal block is transformed by (N_c+N_g)-point discrete Fourier transform (DFT) into the frequency domain signal. The received signals from all distributed antennas are collected to the SPC and the QRM-MLBD is carried out to output log likelihood ratio (LLR). Finally, channel decoding is performed by using the LLR output to recover the transmit data sequence.

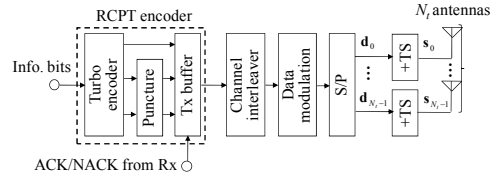

(a) Transmitter (MT).

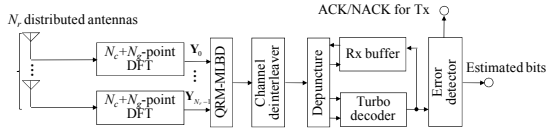

(b) Receiver (SPC).

Figure 3. Transmission system model of SC-MIMO HARQ using QRM-MLBD.

B. Received Signal Representation

Assuming a multi-cell environment, the center cell (c=0) is assumed to be the cell of interest and another cells (c=1~18) is assumed to be the CCI cells. The frequency-domain received signal vector at the m-th receive antenna in the cell of interest $\mathbf{Y}_m^{(0)}=[Y_m^{(0)}(0),...,Y_m^{(0)}(k),...,Y_m^{(0)}(N_c+N_g-1)]^T$, m=0~(N_r–1), after (N_c+N_g)-point DFT is expressed as

$$\mathbf{Y}_m^{(0)} = \sqrt{\frac{2E_s}{T_sN_t}}\sum_{n=0}^{N_t-1}\mathbf{H}_{m,n}^{(0)}\mathbf{F}\mathbf{s}_n^{(0)}+\mathbf{I}_m+\mathbf{N}_m, \tag{3}$$

where E_s is the total transmit energy normalized by the cell radius R and T_s is the symbol duration. $\mathbf{H}_{m,n}^{(0)}$ is the frequency-domain channel matrix between the n-th transmit antenna and the m-th receive antenna in the cell of interest and is given by

$$\mathbf{H}_{m,n}^{(0)} = diag[H_{m,n}^{(0)}(0),\ldots,H_{m,n}^{(0)}(k),...,H_{m,n}^{(0)}(N_c+N_g-1)], \tag{4}$$

where $H_{m,n}^{(0)}(k)$, k=0~N_c+N_g–1, is the channel gain at the k-th frequency and is given by

$$H_{m,n}^{(0)}(k)=\sqrt{r_m^{(0)-\alpha}\cdot 10^{-\eta_m^{(0)}/10}}\sum_{l=0}^{L-1}h_{m,n,l}^{(0)}\exp\left(-j2\pi k\frac{\tau_{m,n,l}^{(0)}}{N_c+N_g}\right). \tag{5}$$

$\mathbf{F}$ is the DFT matrix of size (N_c+N_g)×(N_c+N_g) [8], $\mathbf{I}_m=[I_m(0),\ldots,I_m(k),\ldots,I_m(N_c+N_g-1)]^T$ is the CCI vector, and $\mathbf{N}_m=[N_m(0),\ldots,N_m(k),\ldots,N_m(N_c+N_g-1)]^T$ is the noise vector whose element is the zero-mean additive white Gaussian noise (AWGN) having the variance $2N_0/T_s$ with N_0 being the one-sided power spectrum density. In the case of a single-cell environment, $\mathbf{I}_m$=0 while in the case of a multi-cell environment, the element of $\mathbf{I}_m$ is expressed as

$$I_m(k)=\frac{1}{\sqrt{N_c+N_g}}\sum_{t=0}^{N_c+N_g-1}i_m(t)\exp\left(-j2\pi k\frac{\tau_{m,n,l}^{(0)}}{N_c+N_g}\right), \tag{6}$$

where

$$i_m(t)=\sqrt{\frac{2E_s}{T_sN_t}}\sum_{c=1}^{18}\sqrt{r_m^{(c)-\alpha}\cdot 10^{-\eta_m^{(c)}/10}}\sum_{n=0}^{N_t-1}\sum_{l=0}^{L-1}h_{m,n,l}^{(c)}s_n^{(c)}(t-\tau_{m,n,l}^{(c)}). \tag{7}$$

$r_m^{(c)}$ and $\eta_m^{(c)}$ are respectively the normalized distance and shadowing loss between the MT in the c-th cell and the m-th distributed antennas in the cell of interest. $h_{m,n,l}^{(c)}$ and $\tau_{m,n,l}^{(c)}$ are respectively the path gain and the time delay of the l-th path between the n-th transmit antenna of the MT in the c-th cell and the m-th distributed antenna in the cell of interest. Since $\mathbf{I}_m(k)$ is the sum of the independent CCI from many MTs in the neighboring cells, the CCI plus noise can be approximated as a complex-valued Gaussian variable as $G_m(k)\equiv I_m(k)+N_m(k)$. The variance $2\sigma_m^2$ of $G_m(k)$ is expressed as

$$2\sigma_m^2=\frac{2E_s}{T_s}\sum_{c=1}^{18}r_m^{(c)-\alpha}\cdot 10^{-\eta_m^{(c)}/10}+\frac{2N_0}{T_s}. \tag{8}$$

C. QRM-MLBD

From Eqs. (3) and (8), the N_r(N_c+N_g)×1 overall frequency-domain received signal $\overline{\mathbf{Y}}$ is given by (the index (0) is omitted for the sake of simplicity)

$$\begin{aligned}\overline{\mathbf{Y}} &= \begin{bmatrix}\mathbf{Y}_0/\sqrt{2\sigma_0^2}\\ \vdots \\ \mathbf{Y}_{N_r-1}/\sqrt{2\sigma_{N_r-1}^2}\end{bmatrix} = \sqrt{\frac{2E_s}{T_sN_t}}\overline{\mathbf{H}}\begin{bmatrix}\mathbf{s}_0\\ \vdots\\ \mathbf{s}_{N_t-1}\end{bmatrix}+\begin{bmatrix}\mathbf{G}_0/\sqrt{2\sigma_0^2}\\ \vdots\\ \mathbf{G}_{N_r-1}/\sqrt{2\sigma_{N_r-1}^2}\end{bmatrix}, \\ &= \sqrt{\frac{2E_s}{T_sN_t}}\overline{\mathbf{H}}\overline{\mathbf{s}}+\overline{\mathbf{G}}\end{aligned} \tag{9}$$

where $\overline{\mathbf{H}}$ is an equivalent channel matrix of size N_r(N_c+N_g)×N_t(N_c+N_g), which is a concatenation of the space and frequency-domain channel and DFT given by

$$\overline{\mathbf{H}}=\begin{bmatrix}\mathbf{H}_{0,0}\mathbf{F}/\sqrt{2\sigma_0^2} & \cdots & \mathbf{H}_{0,N_t-1}\mathbf{F}/\sqrt{2\sigma_0^2}\\ \vdots & \ddots & \vdots \\ \mathbf{H}_{N_r-1,0}\mathbf{F}/\sqrt{2\sigma_{N_r-1}^2} & \cdots & \mathbf{H}_{N_r-1,N_t-1}\mathbf{F}/\sqrt{2\sigma_{N_r-1}^2}\end{bmatrix}. \tag{10}$$

$\overline{\mathbf{s}}$ is the N_t(N_c+N_g)×1 overall transmit symbol vector and $\overline{\mathbf{G}}$ is the N_r(N_c+N_g)×1 overall CCI+noise vector.

QRM-MLBD consists of three steps; ordering, QR decomposition, and M-algorithm. The ordered overall transmit symbol vector $\overline{\mathbf{s}}^{order}$ can be expressed as

$$\mathbf{s}^{order} = [s_1(0),...,s_{N_t}(0),...,s_1(N_c+N_g-1),...,s_{N_t}(N_c+N_g-1)]^T = [\mathbf{d}^T(0),\mathbf{d}^T(1),...,\mathbf{d}^T(N_c-1),\mathbf{u}^T(0),...,\mathbf{u}^T(N_g-1)]^T \quad (11)$$

where $\mathbf{d}^T(t)$ and $\mathbf{u}^T(t)$ denote the data symbol vector and TS vector at t-th symbol of size $N_t \times 1$, respectively. After ordering, QR decomposition is applied to the ordered equivalent channel matrix to obtain $\overline{\mathbf{H}} = \mathbf{QR}$, where $\mathbf{Q}$ is an $N_r(N_c+N_g) \times N_t(N_c+N_g)$ unitary matrix and $\mathbf{R}$ is an $N_t(N_c+N_g) \times N_t(N_c+N_g)$ upper triangular matrix. The transformed received signal $\hat{\mathbf{Y}}$ is obtained as

$$\hat{\mathbf{Y}} = \mathbf{Q}^H \overline{\mathbf{Y}} = \sqrt{\frac{2E_s}{T_s N_t}} \mathbf{R} \bar{\mathbf{s}}^{order} + \mathbf{Q}^H \overline{\mathbf{G}} . \quad (12)$$

From Eq. (12), the ML solution is equivalent to the selection of the path with the minimum Euclidean distance in the tree diagram which is composed of $N_t(N_c+N_g)$ stages. In each stage, the best M surviving paths are selected based on the squared Euclidean distance from all the paths and are passed to the next stage. The obtained bit LLRs are used as the input to the channel decoder. When M-algorithm is used, however, the LLR values cannot be directly computed since surviving paths at the last stage may not contain both 1 and 0 for every coded bit. In this paper, we applied the LLR computation method proposed in [19].

It can be understood from Eqs. (11) and (12) that in TS-SC MIMO multiplexing with ordering, TSs are localized at the bottom of the overall transmit signal vector of size $N_t(N_c+N_g) \times 1$. This helps to improve the detection performance of the MLD using M-algorithm. In the case of SC-MIMO block transmissions, the magnitude of a complex-valued element closer to the lower right positions of matrix $\mathbf{R}$ may drop with higher probability. The received signal powers associated with symbols to be detected at early stages in the M-algorithm significantly drop and hence, the probability of removing the correct path at early stages may increase when a smaller M is used. However, in TS-SC MIMO multiplexing, the symbols to be detected at early stages in the M-algorithm are symbols belonging to the known TSs. Therefore, the probability of removing the correct path can be significantly reduced even if small M is used.

IV. Computer Simulation

A. Simulation Condition

Computer simulations are done to measure the uplink throughput distributions of DAN and CN, both of which use SC-MIMO HARQ with QRM-MLBD. The simulation condition is summarized in Table I. 16QAM is assumed for data modulation. We assume N_t=N_r=2, N_c=64, N_g=16, and L=16-path frequency-selective block Rayleigh fading channel with exponential power delay profile having the decay factor 3dB. Independent channel is assumed for each retransmission. The ideal channel estimation is assumed at the receiver (SPC). A rate 1/3 turbo encoder using two (13, 15) recursive systematic convolutional (RSC) component encoders is used for channel encoder. We apply HARQ type-II S-P4 strategy. Log-MAP decoding with 6 iterations is used. The packet size is set to 2048 bits. An error-free ACK/NACK feedback is assumed from the receiver to MT.

We measured the throughput by changing the MT's location randomly to find the cumulative distribution function (CDF) of the throughput. A single MT is assumed. From the CDF, the 10% and 50%-outage throughputs, below which the throughput falls at a probability of 10% or 50%, are obtained.

TABLE I. Computer Simulation Condition

Channel coding	R_c=1/3 (13, 15) RSC encoder Log-MAP decoding with 6 iterations	
HARQ	HARQ type II S-P4	
Transmitter	Data modulation	16QAM
	No. of transmit antennas	N_t=2
	Data symbol block length	N_c=64
	TS lengths	N_g=16
Channel	Fading type	Frequency-selective block Rayleigh
	Power delay profile	L=16 path exponential power delay profile
	Decay factor	3dB
	Path loss exponent	α=3.5
	Shadowing loss standard deviation	σ=7.0
Receiver	No. of antennas in a cell	N_{total}=7
	No. of receive antennas	N_r=2
	Channel estimation	Ideal

B. Single-Cell Environment

The spatial distribution of the measured throughput in DAN and CN is illustrated in Fig. 4 for the normalized transmit E_s/N_0=5dB. QRM-MLBD with M=4 is used for the signal detection. It can be clearly seen from Fig. 4 that DAN achieves much higher throughput over an entire cell; the throughput at the cell edge is about 5.5 (bps/Hz) in DAN while it is about 1.5 (bps/Hz) in CN. This is because DAN can mitigate the negative impact arising from path and shadowing losses by using distributed antennas. In the CN, however, the throughput at the cell edge significantly drops because all the antennas suffer from the same path loss and shadowing effects.

Figure 5 plots the 10% and 50% outage throughputs of DAN and CN. QRM-MLBD with M=4 and 16 is used for the signal detection. For comparison, the 10% and 50% outage throughputs in DAN and CN using MMSED are also plotted. We can see from Fig. 5 that DAN achieves significantly higher 10% and 50% outage throughput than CN. This is because, in DAN, distributed antennas near the MT can be chosen and hence, the impact of path loss can be significantly suppressed. We compare the required normalized transmit E_s/N_0 for achieving 10% and 50% throughputs of 6.38bps/Hz. In DAN, the required normalized transmit E_s/N_0 for 10(50)% outage throughput of 6.38bps/Hz can be reduced by about 14(10)dB compared to CN.

We can also see from Fig. 5 that QRM-MLBD can improve the throughput compared to the MMSED. The E_s/N_0 reduction from MMSED for 10% outage throughput of 6.38bps/Hz is as much as about 18dB in DAN.

C. Multi-Cell Environment

Figure 6 shows the 10% and 50% outage throughputs normalized by the frequency reuse factor F in DAN and CN as a function of the frequency reuse factor F. The normalized total transmit E_s/N_0 is set to infinite (i.e., an interference limited environment). QRM-MLBD with M=4 and 16 is used for the signal detection. For comparison, the 10% and 50% outage

throughputs in DAN and CN using MMSED are also plotted. We can see from Fig. 6 that DAN achieves significantly higher 10% and 50% outage throughput than CN. This is because, in DAN, distributed antennas near the MT can be chosen and hence, the impact of path loss can be significantly suppressed.

In CN, the 10% outage throughput is maximized when F=7 because strong CCI exists when F is smaller. However, in DAN, the 10% outage throughput can be maximized when F=1 or 3. This is because, in DAN, the received SINR can be increased without increasing F.

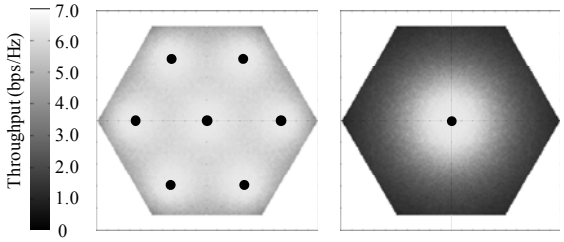

(a) DAN. (b) CN.

Figure 4. Spatial distribution of throughput.

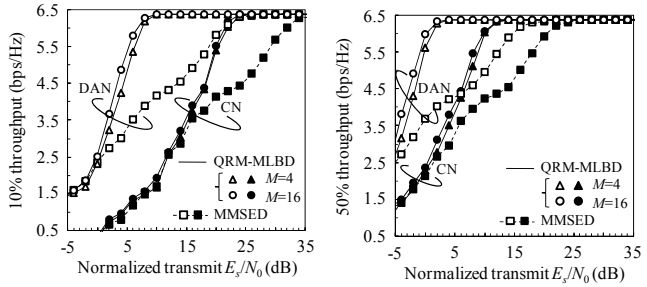

(a) 10% outage throughput. (b) 50% outage throughput.

Figure 5. Outage throughput.

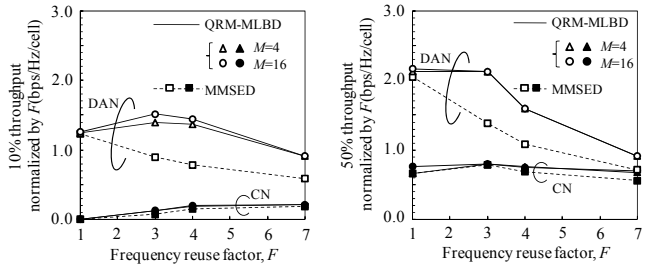

(a) 10% outage throughput. (b) 50% outage throughput.

Figure 6. Outage throughput normalized by the frequency reuse factor.

V. CONCLUSION

In this paper, we investigated the uplink throughput of DAN using SC-MIMO packet transmission employing type II HARQ and QRM-MLBD. First, we compared DAN-MIMO and CN-MIMO in terms of the uplink throughput distribution in a single-cell environment. We showed that DAN achieves higher throughput over the entire cell and significantly reduces the transmit power for achieving the required throughput compared to CN. Then, we compared DAN-MIMO and CN-MIMO in a multi-cell environment and showed that DAN significantly improves the spectrum efficiency compared to CN.

REFERENCES

[1] G. J. Foschini and M. J. Gans, "On limits of wireless communications in a fading environment when using multiple antennas," Wireless Personal Commun., Vol. 6, No. 3, pp. 311-335, 1998.

[2] H. Ekstrom, A. Furuskar, J. Karlsson, M. Meyer, S. Parkvall, J. Torsner, and M. Wahlqvist, "Technical solutions for the 3G long-term evolution," IEEE Commun. Mag., Vol. 44, No. 3, pp. 38-45, Mar. 2006.

[3] N. Benjamin, L. Chan-Tong, and D. Falconer, "Trubo frequency domain equalization for single-carrier broadband wireless systems," IEEE Trans. on Wireless Commun., Vol. 6, No. 2, pp. 759-767, Feb. 2007.

[4] K. Higuchi, H. Kawai, N. Maeda, H. Taoka, and M, Sawahashi, "Experiments on real-time 1-Gb/s packet transmission using MLD-based signal detection in MIMO-OFDM broadband radio access," IEEE J. Selected Areas in Commun., Vol. 24, No. 6, pp. 1141-1153, June 2006.

[5] 3GPP, PR-050758, "LS on UTRAN LTE multiple access selection," Nov. 2005.

[6] J. G. Proakis and M. Salehi, *Digital communications*, 5th ed., McGraw-Hill, 2008.

[7] Nagatomi, K. Higuchi, and H. Kawai, "Complexity reduced MLD based on QR decomposition in OFDM MIMO multiplexing with frequency domain spreading and code multiplexing," Proc. IEEE Wireless Communications and Networking Conference (WCNC 2009), Apr. 2009.

[8] T. Yamamoto, K. Takeda, and F. Adachi, "Training sequence-aided QRM-MLD block signal detection for single-carrier MIMO spatial multiplexing," Proc. IEEE International Conference on Communications (ICC 2011), June 2011.

[9] T. Yamamoto and F. Adachi, "HARQ throughput performance of training sequence aided SC-MIMO using reduced complexity ML block detection," Proc. IEEE 75th Vehicular Technology Conference (VTC2012-Spring), May 2012.

[10] A. A. M. Saleh, A. J. Rustako, and R. S. Roman, "Distributed antennas for indoor radio communications," IEEE Trans. Commun., Vol. 35, No. 12, pp. 1245-1251, Dec. 1987.

[11] H. Hu, Y. Zhang, and Y. Yao, *Distributed antenna systems; open architecture for future wireless communications*, Auerbach Pub., 2007.

[12] F. Adachi, K. Takeda, T. Yamamoto, R. Matsukawa, and S. Kumagai, "Recent advances in single-carrier distributed antenna network," Wireless Communications and Mobile Computing, Vol. 11, No. 12, pp. 1551–1563, Dec. 2011.

[13] S. Kumagai, R. Matsukawa, T. Obara, T. Yamamoto, and F. Adachi, "Channel capacity improvement of MIMO spatial multiplexing on distributed antenna network," IEICE Technical Report, RCS2011-144, Oct. 2011.

[14] S. Kumagai, R. Matsukawa, T. Obara, T. Yamamoto, and F. Adachi, "Spectrum efficiency of distributed antenna network using MIMO spatial multiplexing," to be presented at IEEE 76th Vehicular Technology Conference (VTC2012-Fall), Sept. 2012.

[15] D. N. Rowitch and L. B. Milstein, "Rate compatible punctured turbo (RCPT) codes in hybrid FEC/ARQ system," Proc. Comm. Theory Mini-conference of GLOBECOM'97, Nov. 1997.

[16] D. Garg and F. Adachi, "Throughput comparison of turbo-coded HARQ in OFDM, MC-CDMA and DS-CDMA with frequency-domain equalization," IEICE Trans. Commun., Vol. E88-B, No.2, pp.664-677, Feb. 2005.

[17] L. Deneire, B. Gyselinckx, and M. Engels, "Training sequence versus cyclic prefix - a new look on single carrier communication," IEEE Commun. Lett., Vol. 5, No. 7, pp. 292-294, July 2001.

[18] F. Adachi, T. Obara, and T. Yamamoto, "Capacity and BER performance considerations on single-carrier frequency-domain equalization," Proc. The 8th International Conference on Information, Communications, and Signal Processing (ICICS 2011), Dec. 2011.

[19] W. Shin, H. Kim, M Son, and H. Park, "An improved LLR computation for QRM-MLD in coded MIMO systems," Proc. IEEE 66th Vehicular Technology Conference (VTC2007-Fall), pp.447-451, 30 Sept. - 3 Oct. 2007.